Journal of Materials Chemistry A

ROYAL SOCIETY OF CHEMISTRY

PAPER

View Article Online
View Journal | View Issue





Cite this: *J. Mater. Chem. A*, 2021, **9**, 4075

# Constructing a robust gigantic drum-like hydrophobic $[Co_{24}U_6]$ nanocage in a metal–organic framework for high-performance $SO_2$ removal in humid conditions†

Yaling Fan,[a] Mengjia Yin,[a] Rajamani Krishna,[b] Xuefeng Feng[a] and Feng Luo *[a]

Received 14th October 2020
Accepted 30th December 2020

DOI: 10.1039/d0ta10004h

rsc.li/materials-a

Constructing a gigantic hydrophobic metal–organic cage is not only scientifically important, but also synthetically challenging. Little is still known about the one the self-assembly and succedent host–guest recognition of transitional-metal-actinides cages. Herein, we report an unprecedented gigantic transitional-metal-uranyl $[Co_{24}U_6]$ drum-like nanocage templated by a propyl-fused imidazolate dicarboxylate ligand. This nanocage-based MOF (namely **Cage-U-Co-MOF**) shows a high thermal and chemical stability in water and weak acidic/alkaline solution, as well as an impressively hydrophobic nature. More importantly, the breakthrough test on the **Cage-U-Co-MOF** bed disclosed this material as a highly effective and selective adsorbent for the removal of trace $SO_2$ (ppm level) from $SO_2/CO_2$ or $SO_2/CO_2/N_2$ mixture under both drying and humid conditions, which suggests its superior application in industrial desulfurization. This work outlines a fundamental molecule-designing concept for preparing hydrophobic transitional-metal-actinides cages for advanced host–guest recognition.

## Introduction

Cage compounds, including organic cages and coordination-driven cages, are a unique species because of their inherent permanent porosity that shows myriad applications, including host–guest chemistries, molecular recognition and separation, and catalysis, as well as biomedical applications.[1–6] Among this category, deliberately constructing hydrophobic cage compounds is expressly important for certain special tasks that could not be achieved by common materials, although it is still a synthetically challenging issue. However, anchoring actinides into cage compounds is extremely interesting and intriguing, which will not only deeply disclose the self-assembly and coordination rule of actinides, thus seeking out a new solution for actinides separation but also shows us some uniqueness in the aspect of aesthetics or function.

Recently, cage have been known as powerful secondary building blocks for constructing cage-based metal–organic frameworks (MOFs).[7–12] This new category not only has the unique feature of inherent permanent porosity from cages but also has the highly regular arrangement of cages that could to some extent enhance host–guest interactions. Moreover, cage-based MOFs often show higher chemical and thermal stability than pure cage compounds. All these merits are indicative of their superior application in catalysis and separation. For example, Li *et al.* recently reported a $Ni_{24}$-cage-based mesoporous MOF, which enables high catalytic performance for carbon–carbon coupling.[13] Zhao *et al.* used a $Zn_{116}$ cage-based MOF to implement noble-metal-free conversion of propargylic amines and $CO_2$.[9] Furthermore, cage-based MOFs were reported to be very effective for selective adsorption of $SO_2$ over $CO_2$ and $N_2$, which suggests their promising application in flue gas desulfurization (FGD) process.[14] However, the humidity, which is close to the real condition of FGD process, will not only significantly decrease the desulfurization ability but also inevitably destroy the structure of MOF material because of the strong acidity of $SO_2$ in humid conditions.

Herein, we reported the synthesis and structure of a gigantic $[Co_{24}U_6]$ nanocage-based MOF (**Cage-U-Co-MOF**). A drum-like configuration was observed for this $[Co_{24}U_6]$ nanocage with two drum planes up and down made by a $Co_6$ cluster and the middle bulgy section made by a $Co_{12}$ cluster, where their formation was templated by propyl groups of organic ligands, which thus leads to the hydrophobic nature. The validity of selective adsorption of $SO_2$ over $CO_2$ and $N_2$ under both drying and humid conditions was confirmed *via* breakthrough experiments.

[a]*School of Chemistry, Biology and Materials Science, East China University of Technology, Nanchang 330013, P. R. China. E-mail: ecitluofeng@163.com*

[b]*Van't Hoff Institute for Molecular Sciences, University of Amsterdam, Science Park 904, 1098 XH Amsterdam, The Netherlands*

† Electronic supplementary information (ESI) available. CCDC 2032794. For ESI and crystallographic data in CIF or other electronic format see DOI: 10.1039/d0ta10004h

# Experimental

### Materials and physical measurements

All chemicals were directly purchased from Innochem without further purification. The data of X-ray powder diffraction were collected on a Bruker AXSD8 Discover powder diffractometer at 40 kV/40 mA for CuKα ($\lambda = 1.5406$ Å) at room temperature in the range of 5–50° ($2\theta$) with a scan speed of 0.1° per step. Thermogravimetric analysis (TGA) was performed by a TGA Q500 thermal analysis system. All TGA experiments were performed under a $N_2$ atmosphere from 40 to 800 °C at a rate of 5 °C $min^{-1}$. The gas sorption isotherms were collected on ASAP2020 PLUS (anti-corrosion version). Ultrahigh-purity-grade (>99.999%) $N_2$, Ar, $CO_2$, and $SO_2$ gases were used in this adsorption measurement. To maintain the experimental temperatures, liquid nitrogen (77 K), liquid argon (87 K), and temperature-programmed water bath (273 and 298 K) were used.

### Synthesis of Cage-U-Co-MOF

2-Propyl-2*H*-imidazole-4,5-dicarboxylic acid (0.1 mmol, 19 mg), uranyl nitrate (0.1 mmol, 50 mg), $Co(NO_3)_2$ (0.1 mmol, 29 mg) were dissolved in a mixture of 2 mL $H_2O$ and 3 mL DMF in the presence of concentrated nitric acid (0.1 mL). The solution was moved into a 25 mL Teflon-lined stainless steel vessel and heated at 120 °C for 3 days. Then, it was cooled to room temperature. Red crystals were filtered and washed with 10 mL of methyl alcohol and 10 mL of deionized water.

### Degassing Cage-U-Co-MOF

100 mg of MOF crystals were soaked in methanol for 3 days and fresh methanol was added every 8 h. After decanting the methanol extract, the sample was dried at room temperature overnight, and then further degassed using ASAP2020 PLUS for 24 h at 200 °C.

# Results and discussion

### Structure of Cage-U-Co-MOF

MOF, $[(UO_2)_6Co_{11}(H_2O)_{18}(L)_{12}][NH_2(CH_3)_2]_2$, was synthesized by a solvothermal reaction of $UO_2(NO_3)_2$, $Co(NO_3)_2$, and L ligand (2-propyl-2*H*-imidazole-4,5-dicarboxylic acid). The structure was determined by a single-crystal X-ray diffraction and the phase purity of the bulk samples was confirmed by powder X-ray diffraction (PXRD). The MOF shows high symmetry with trigonal crystal system and space group of *P*31*c*, which contains two crystallography independent uranyl ions and five crystallography independent cobalt ions. Both U1 and U2 sites afford the seven-coordinated distorted pentagonal bipyramid configuration, finished by two uranyl oxygen atoms, four carboxylate oxygens from two $L^{3-}$ ligands, plus one terminal water molecule (potential open-metal sites for recognition of guest molecule). The U–O bond lengths ranging from 1.668(18) Å to 2.486(15) Å are in the normal range.[16] Two distinct coordination modes observed for Co sites, where $Co_1$ and $Co_5$ sites display the five-coordinated distorted pyramidal geometry made by two

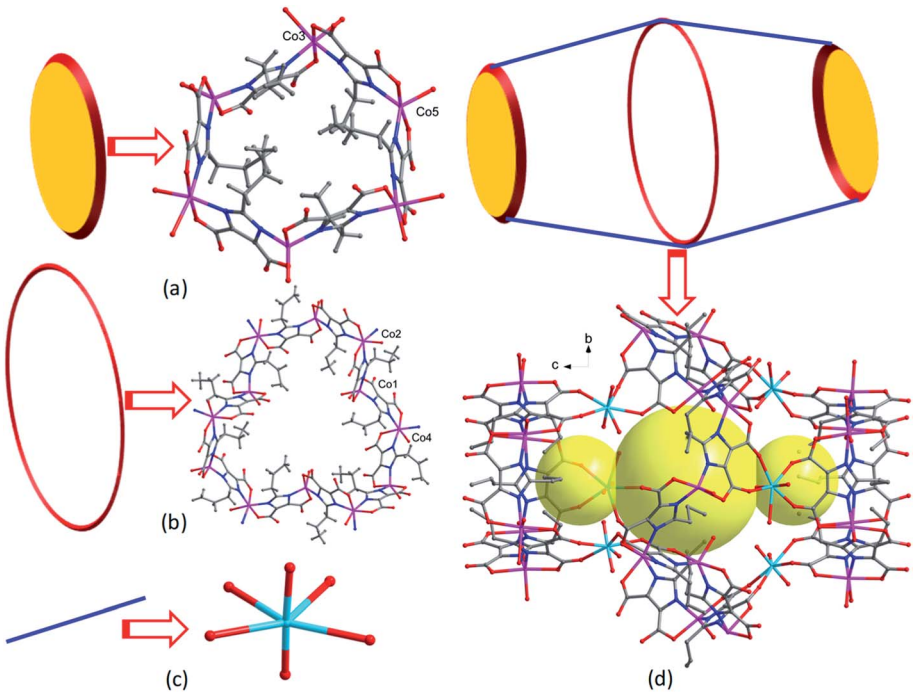


Fig. 1 View of the hydrophobic drum-like $Co_{24}U_6$ cage. (a) One of the drum planes for the drum-like $Co_{24}U_6$ cage formed by six Co(II) ions and six $L^{3-}$ ligands. (b) The middle bulge of drum formed by twelve Co(II) ions and twelve $L^{3-}$ ligands. (c) The $UO_2$ linkers that locate at the skeleton of drum and act as linker to bridge $Co_6$ cluster and $Co_{12}$ cluster. (d) Ball-and-stick structure and schematic description of this unique hydrophobic drum-like $Co_{24}U_6$ cage with the solvent-accessible pore highlighted by light yellow ball (the bigger and smaller balls present the bigger and smaller pores in this drum-like $Co_{24}U_6$ cage).

 

oxygens and two nitrogens from two $L^{3-}$ ligands, as well as one terminal water molecule, which indicates potential open-metal sites for recognition of guest molecules, whereas $Co_2$, $Co_3$, and $Co_4$ sites hold six-coordinated octahedral geometry composed of three oxygens and three nitrogens from three $L^{3-}$ ligands. Each $L^{3-}$ ligands connect to two Co ions and one uranyl ion through carboxylate and imidazole units.

The outstanding structure feature of this MOF is the $Co_{24}U_6$ cage. As shown in Fig. 1a, $Co_3$, $Co_5$, and symmetry-related counterparts were combined together by six $L^{3-}$ ligands which creates a planar $Co_6$ hexagon cluster. While $Co_1$, $Co_2$, and $Co_4$, as well as symmetry-related counterparts were connected by twelve $L^{3-}$ ligands, which generates a planar $Co_{12}$ cluster (Fig. 1b). Interestingly, all the propyl groups from $L^{3-}$ ligands in both $Co_6$ and $Co_{12}$ clusters are located in the ring of $Co_6$ and $Co_{12}$ cluster and point to its center, which strongly suggests that the formation of $Co_6$ and $Co_{12}$ cluster was primarily induced by propyl templates from $L^{3-}$ ligands, consequently implying their potential hydrophobic nature. Through six uranyl ions, two identical $Co_6$ clusters and one $Co_{12}$ cluster are connected, which constructs a gigantic $Co_{24}U_6$ cage with drum-like configuration, where two identical $Co_6$ clusters act as two drum planes and one $Co_{12}$ cluster plays a role in the middle bulge of the drum

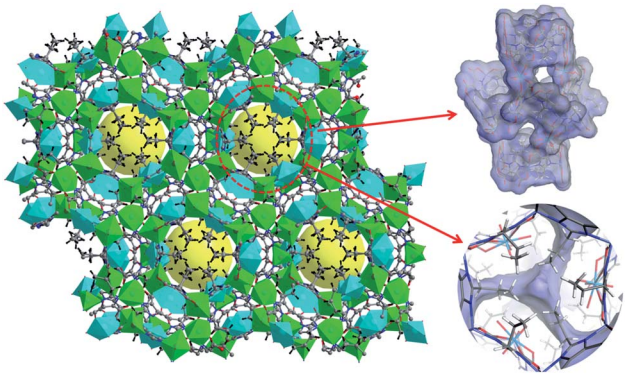

Fig. 2 View of the 3D net of **Cage-U-Co-MOF** with the highlighted section of porous $Co_{24}U_6$ cage and the pore configuration of the $Co_{24}U_6$ cage.

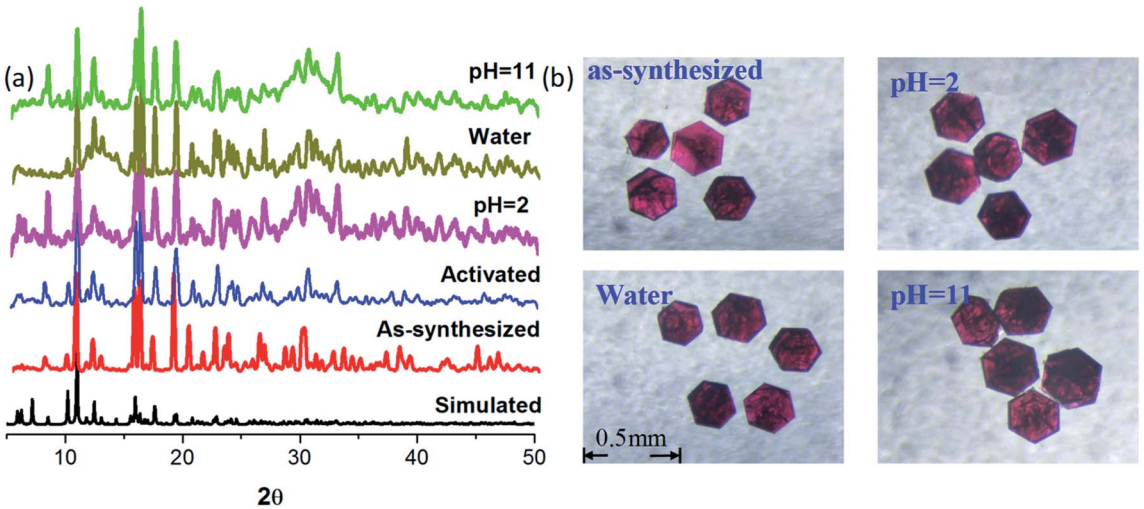


Fig. 3 (a) A comparison of PXRD patterns among the one simulated from single crystal data, and as-synthesized samples, degassed samples after 200 °C calcination, samples after immersing in water and pH = 2/11 solution for one week. (b) The photograph of **Cage-U-Co-MOF** crystals under different surroundings (water and pH = 2/11 solution for one week).

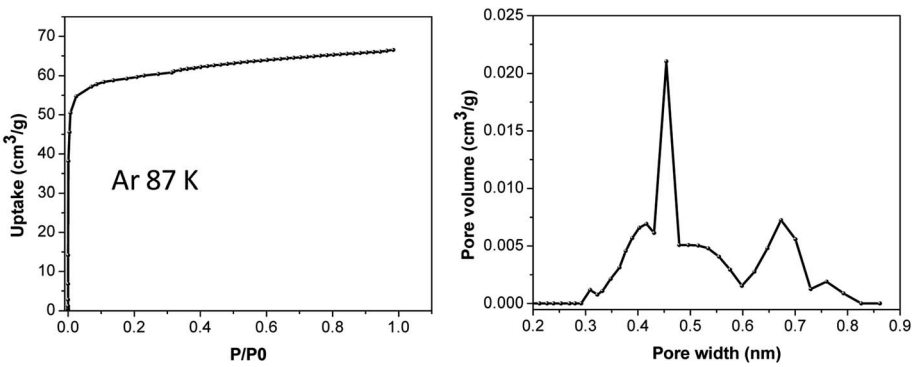


Fig. 4 Ar adsorption at 87 K for **Cage-U-Co-MOF** and the pore distribution.

together with six uranyl ions, which are located on the skeleton of the drum. As we know, actinides, especially uranyl ions, were explored to generate cage compounds through coordination with oxide, peroxide, or hydroxide groups.[6b] However, 3d–5f bimetal cage-based MOF are quite rare. Due to the special drum-like configuration, the $Co_{24}U_6$ cage shows a bigger aperture of *ca.* 0.72 nm in the middle section (Fig. 1d, bigger yellow ball) and smaller aperture of *ca.* 0.4 nm in the terminal section (Fig. 1d, smaller yellow ball). The size of the $Co_{24}U_6$ cage is up to 2.2 nm × 1.6 nm. Fig. 2 shows the 3D net of **Cage-U-Co-MOF** was shown, where the solvent-accessible volume, estimated by Platon program, is 45.3% of the cell volume,[15] which suggests potential porosity.

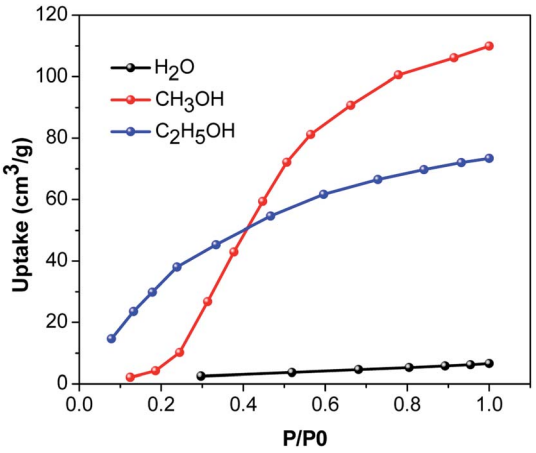


Fig. 5 The adsorption isotherms of $H_2O$, $CH_3OH$ and $C_2H_5OH$ on **Cage-U-Co-MOF** at room temperature.

### Characterization of Cage-U-Co-MOF

Firstly, the thermal stability of this material was evaluated by TG analysis (Fig. S1†). For pristine samples, we cannot estimate its thermal stability due to the continuous weight loss at 30–450 °C. However, a stable platform can be observed for the $CH_3OH$-exchanged samples, where the loss of solvent molecules is before 200 °C. The PXRD patterns of the $CH_3OH$-exchanged samples after calcining at 200 °C for 24 agrees with that observed in as-synthesized samples (Fig. 3a), which suggests the high thermal stability of **Cage-U-Co-MOF**. Accordingly, the degassing temperature was set at 200 °C. Chemical stability was further investigated. Impressively, under water and weak acidic and alkaline conditions (pH = 2 and pH = 11) the crystals of **Cage-U-Co-MOF** were maintained for about one week without any breakage (Fig. 3b). This was further confirmed by comparing the XRD patterns and Ar adsorption of as-synthesized samples with the samples after immersing in water and weak acidic and alkaline solution for one week

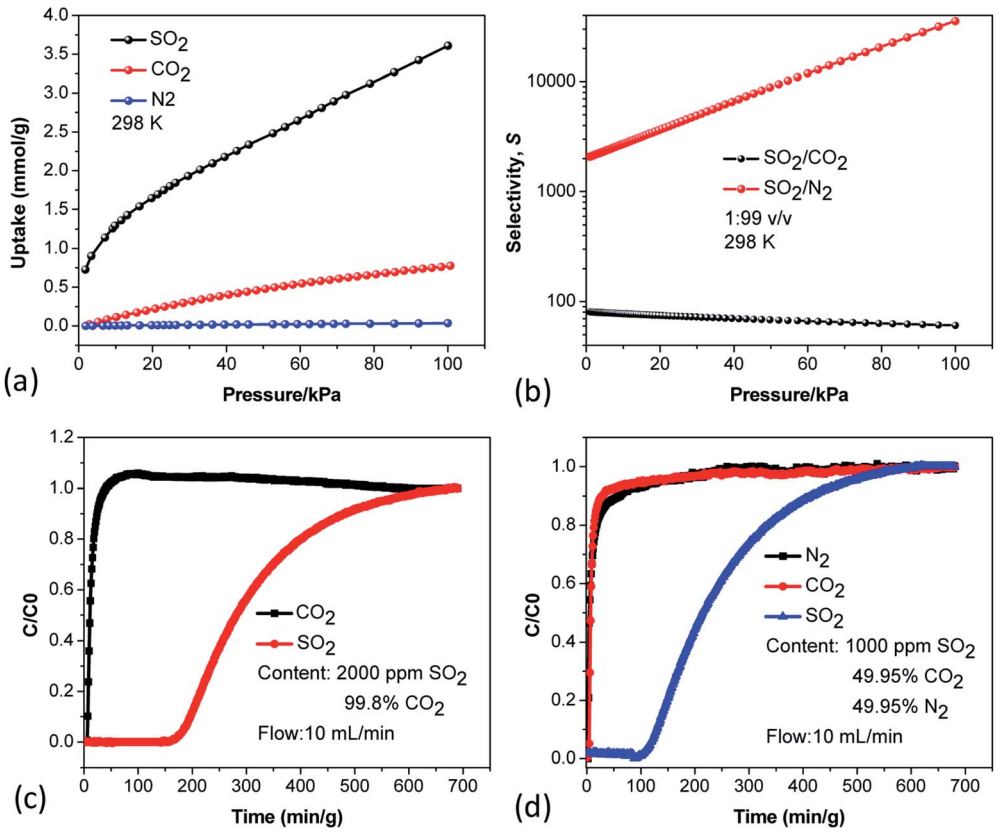


Fig. 6 (a) The $SO_2$, $CO_2$ and $N_2$ adsorption isotherms at 298 K. (b) The $SO_2$ adsorption selectivity over $CO_2$ and $N_2$ for a 1 : 99 v/v $SO_2/CO_2$ or $SO_2/N_2$ mixture. (c) Breakthrough experiments based on **Cage-U-Co-MOF** bed (0.5 g) under a 10 mL $min^{-1}$ flow for $SO_2/CO_2$ mixture. (d) Breakthrough experiments based on **Cage-U-Co-MOF** bed (0.5 g) under a 10 mL $min^{-1}$ flow for the $SO_2/CO_2/N_2$ mixture.

 

(Fig. 3a and S2†). The permanent porosity for the degassed samples was tested by Ar adsorption at 87 K, which gives a typical-I adsorption with Brunauer–Emmett–Teller (BET) surface area of 208 $m^2\ g^{-1}$ that suggests a microporous framework in **Cage-U-Co-MOF** (Fig. 4). The pore distribution is broad from 0.3 nm to 0.8 nm with two major pores at 0.45 nm and 0.69 nm (Fig. 4), respectively, which are comparable with the smaller and bigger pore in this $Co_{24}U_6$ cage. Considering the hydrophobic nature of this $Co_{24}U_6$ cage, we then carried out the test of $H_2O$, $CH_3OH$ and $C_2H_5OH$ adsorption. As shown in Fig. 5, it is clear that almost no adsorption of $H_2O$ (6.5 $cm^3\ g^{-1}$) was observed; however, this MOF enables high $CH_3OH$ and $C_2H_5OH$ adsorption up to 109.9 $cm^3\ g^{-1}$ and 73.4 $cm^3\ g^{-1}$, respectively, which strongly implies the hydrophobic nature of this MOF.[8]

### Removal of $SO_2$ by Cage-U-Co-MOF

Removing $SO_2$ is of great significance in gas-purification processes, including flue-gas desulfurization and natural-gas purification. In contrast to the traditional flue-gas desulfurization (FGD) processes relying on alkaline organic solvents as absorbents, which present an energy- and cost-intensive pathway, porous solid adsorbent-based FGD technique was more desirable, due to its low cost and energy.[17] However, to date, the design of solid adsorbents with high adsorption capacity and selectivity is still very challenging.[18] Most importantly, most solid adsorbents, especially for MOFs, could not survive from $SO_2$ gas, because of its strong acidity and causticity under humid conditions. Therefore, constructing hydrophobic MOF for such use could be a good solution. In this regard, **Cage-U-Co-MOF** could be a good candidate and thus we further tested $SO_2$ uptake. At 1 bar and 298 K, **Cage-U-Co-MOF** gives $SO_2$ uptake of 3.62 mmol $g^{-1}$, which is comparable with some reported porous adsorbent for such use (Table S1†). However, at the same conditions, the $CO_2$ adsorption capacity is very low (just about 0.77 mmol $g^{-1}$), while almost no $N_2$ adsorption (0.035 mmol $g^{-1}$) was observed (Fig. 6a). The results indicate highly selective adsorption of $SO_2$ over $CO_2$ and $N_2$.

Based on these adsorption data, we then calculated the selectivity by ideal adsorbed solution theory (IAST) calculations. For a 1 : 99 v/v $SO_2/CO_2$ mixture, **Cage-U-Co-MOF** enables ultrahigh $SO_2$ selectivity over $CO_2$ up to 80.7–60.8 (Fig. 6b). Notably, the $SO_2/N_2$ selectivity for a 1 : 99 v/v $SO_2/N_2$ mixture is up to 2078.7–35 620 (Fig. 6b). Ultrahigh $SO_2$ selectivity generally suggests strong affinity towards $SO_2$ from MOF. Careful inspection into the structure discloses that $Co_1$, $Co_5$, U1, and U2 contains terminal coordinated water molecules; thus, these atoms can be viewed to be potential open metal sites after withdrawing the coordinated water molecule, which consequently provides abundant and strong affinity towards $SO_2$ *via* coordination interactions. In the literature, binding $SO_2$ on the open-metal site *via* coordination interactions in MOFs have

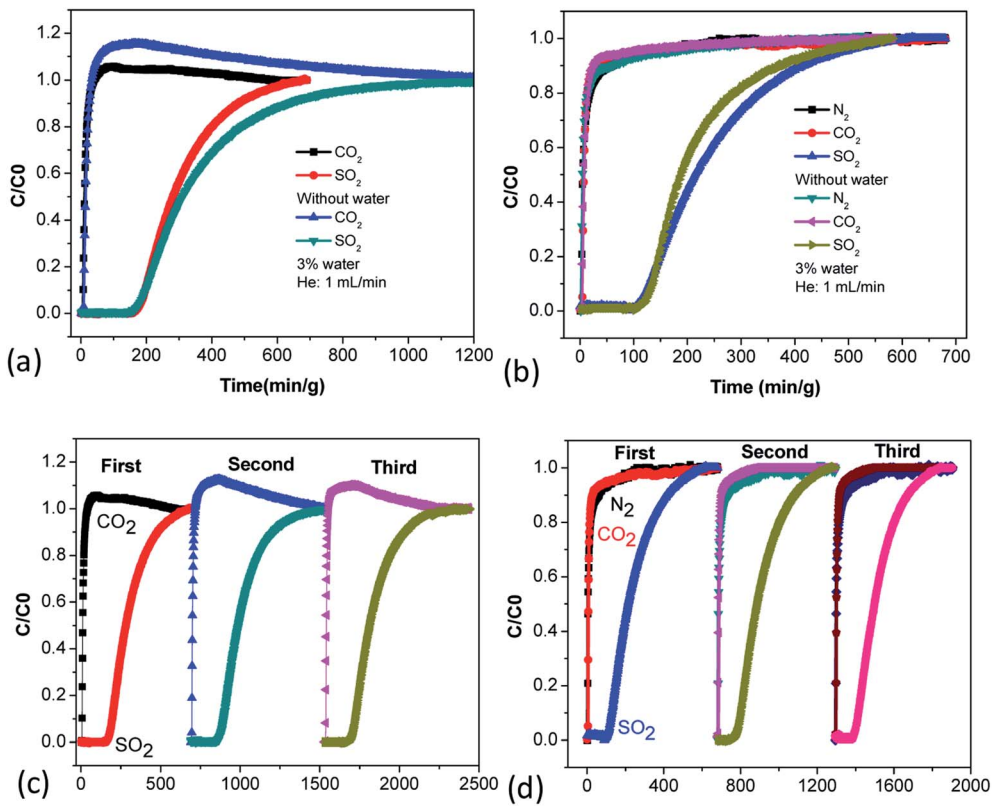


Fig. 7 (a) The recycle use of **Cage-U-Co-MOF** bed for separating $SO_2/CO_2$ mixture. (b) The recycle use of **Cage-U-Co-MOF** bed for separating $SO_2/CO_2/N_2$ mixture. (c) A comparison of separating $SO_2/CO_2$ mixture with or without water. (d) A comparison of separating $SO_2/CO_2/N_2$ mixture with or without water. The water vapor content is 3% in He with a flow of 1 mL $min^{-1}$.

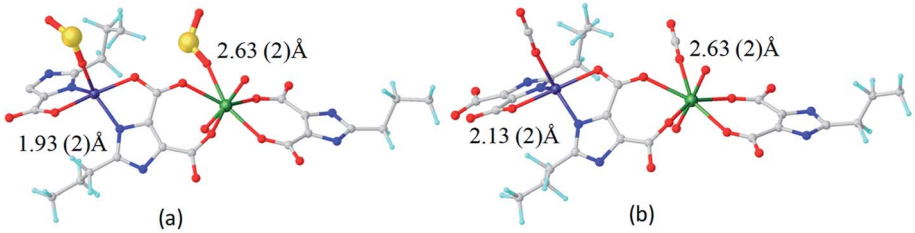


Fig. 8 View of the coordination structure of $SO_2$ and $CO_2$ with the open metal site.

been convincing.[14] The strong affinity towards $SO_2$ from MOF was reflected on the isosteric heats of adsorption ($Q_{st}$), which gives 53.0 kJ $mol^{-1}$ for $SO_2$ and 30.8 kJ $mol^{-1}$ for $CO_2$ at the onset of adsorption (Fig. S3 and S4†), indicative of very strong affinity towards $SO_2$ from the open-metal sites (both Co and U) of MOF.[14,18]

To obtain the $SO_2$ separation ability, we initially performed the transient breakthrough simulations.[19–21] For both 1 : 99 v/v $SO_2/CO_2$ and $SO_2/N_2$ mixture, **Cage-U-Co-MOF** renders excellent $SO_2$ separation (Fig. S5 and S6†). To confirm this at real conditions and meet the practical demand in the FGD process, the $SO_2/CO_2$ mixture, which contains 2000 ppm $SO_2$, was used to carry out breakthrough experiments. $CO_2$ was first eluted after 6 min $g^{-1}$, whereas the breakthrough time of $SO_2$ through **Cage-U-Co-MOF** bed is up to 152 min $g^{-1}$ (Fig. 6c). The huge gap of residence time between $SO_2$ and $CO_2$ confirmed the great potential of **Cage-U-Co-MOF** for removing $SO_2$ in FGD process. As we know, the flue gas is primarily composed of $CO_2$ and $N_2$ and water vapor. Accordingly, we further tested the breakthrough experiments for a ternary $SO_2/CO_2/N_2$ mixture containing 1000 ppm $SO_2$. Complete separation of $SO_2$ from $CO_2$ and $N_2$ was observed, where the residence time of $CO_2$ and $N_2$ was just 3 min $g^{-1}$; however, the corresponding residence time for $SO_2$ was as long as 100 min $g^{-1}$ (Fig. 6d). Furthermore, even under water vapor (3% $H_2O$ in He), the $SO_2$ separation performance from $SO_2/CO_2$ mixture or $SO_2/CO_2/N_2$ mixture was not affected, which is primarily attributed to the hydrophobic nature of the unique $Co_{24}U_6$ cage (Fig. 7a and b). For practical industrial applications, the repeated use of the adsorbent is very important. We found that repeating breakthrough experiments three times from the $SO_2/CO_2$ mixture or $SO_2/CO_2/N_2$ mixture show no decrease in the $SO_2$ separation performance (Fig. 7c and d), while repeating the $SO_2$ adsorption test three times shows no obvious decrease in $SO_2$ uptake (Fig. S7†) and is indicative of its good recycle use. This was further confirmed by comparing PXRD patterns of samples after all these breakthrough experiments with the as-synthesized samples (Fig. S8†) and implies a high chemical stability of **Cage-U-Co-MOF**.

To disclose the adsorption mechanism, we further carried out DFT-D calculations.[22] The binding energy for $SO_2$ with the open U and Co site is −0.36 eV, while the corresponding value for $CO_2$ is −0.12 eV; this suggests higher affinity towards $SO_2$ than $CO_2$ from MOF skeleton and is consistent with experimental results. The Co–O($SO_2$) bond length of 1.93(2) Å is shorter than the Co–O($CO_2$) bond length of 2.13(2) Å, whereas the U–O ($SO_2$) and U–O ($CO_2$) are comparable, *viz.* 2.63(2) Å *vs.* 2.63(2) Å (Fig. 8). Therefore, the excellent selective adsorption of $SO_2$ over $CO_2$ is primarily derived from the open Co site.

## Conclusion

In conclusion, we show in this work a robust unprecedented transitional-metal-actinides MOF composed of gigantic drum-like hydrophobic [$Co_{24}U_6$] nanocage. The self-assembly of such unique cage is primarily templated by the propyl groups of 2-propyl-2*H*-imidazole-4,5-dicarboxylic acid that is a typical N,O-donor ligand and meets the coordination character for both transitional metal ions and actinides ions. The abundant open-metal sites from both transitional metal ions and actinides ions within [$Co_{24}U_6$] nanocage resulted in stronger coordination interaction with $SO_2$, which thus led to a highly selective adsorption of $SO_2$ over $CO_2$ and $N_2$ with outstanding $SO_2/CO_2$ and record $SO_2/N_2$ selectivity. The high chemical stability and hydrophobic nature allows **Cage-U-Co-MOF** with good recycle use and unaffected $SO_2$ separation performance even under humidity conditions, which implies its superior application in FGD process.

## Conflicts of interest

There is no conflict of interest to report.

## Acknowledgements

This work was supported financially by the National Natural Science Foundations of China (21966002, 21871047, 21861017), the Natural Science Foundation of Jiangxi Province of China (20181ACB20003), and the Training Program for Academic and Technical Leaders of Major Disciplines in Jiangxi Province (20194BCJ22010).

## References

1 E. J. Gosselin, C. A. Rowland and E. D. Bloch, *Chem. Rev.*, 2020, **120**, 8987–9014.
2 P. J. Stang and B. Olenyuk, *Acc. Chem. Res.*, 1997, **30**, 502–518.
3 H. Li, Z.-J. Yao, D. Liu and G.-X. Jin, *Coord. Chem. Rev.*, 2015, **293**, 139–157.
4 S. Durot, J. Taesch and V. Heitz, *Chem. Rev.*, 2014, **114**, 8542–8578.

 

5 M. Liu, L. D. Zhang, M. A. Little, V. Kapil, M. Ceriotti, S. Y. Yang, L. F. Ding, D. L. Holden, R. Balderas-Xicohténcatl, D. L. He, R. Clowes, S. Y. Chong, G. Schütz, L. J. Chen, M. Hirscher and A. I. Cooper, *Science*, 2019, **366**, 613–620.

6 (*a*) J. H. Park, Y. P. Chen, Z. Perry, J. R. Li and H. C. Zhou, *J. Am. Chem. Soc.*, 2014, **136**, 16895–16901; (*b*) J. Qiu and P. C. Burns, *Chem. Rev.*, 2013, **113**, 1097–1120.

7 Y. H. Kang, X. D. Liu, N. Yan, Y. Jiang, X. Q. Liu, L. B. Sun and J. R. Li, *J. Am. Chem. Soc.*, 2016, **138**, 6099–6102.

8 C. Wang, D. D. Zhou, Y. W. Gan, X. W. Zhang, Z. M. Ye and J. P. Zhang, *Natl. Sci. Rev.*, 2020, DOI: 10.1093/nsr/nwaa094.

9 C. S. Cao, S. M. Xia, Z. J. Song, H. Xu, Y. Shi, L. N. He, P. Cheng and B. Zhao, *Angew. Chem., Int. Ed.*, 2020, **59**, 8586–8593.

10 X. F. Wang, Y. Y. Chen, L. P. Song, Z. Fang, J. Zhang, F. N. Shi, Y. W. Lin, Y. K. Sun, Y. B. Zhang and J. Rocha, *Angew. Chem., Int. Ed.*, 2019, **58**, 18808–18812.

11 X. J. Hu, Z. X. Li, H. Xue, X. S. Huang, R. Cao and T. F. Liu, *CCS Chem.*, 2019, **1**, 561–570.

12 Y. J. Chen, X. Q. Huang, Y. F. Chen, Y. R. Wang, H. C. Zhang, C. X. Li, L. Zhang, H. J. Zhu, R. X. Yang, Y. H. Kan, S. L. Li and Y. Q. Lan, *CCS Chem.*, 2019, **1**, 561–570.

13 T. He, Z. H. Huang, S. Yuan, X. L. Lv, X. J. Kong, X. D. Zou, H. C. Zhou and J. R. Li, *J. Am. Chem. Soc.*, 2020, **142**, 13491–13499.

14 G. L. Smith, J. E. Eyley, X. Han, X. R. Zhang, J. N. Li, N. M. Jacques, H. G. W. Godfrey, S. P. Argent, L. J. McCormick McPherson, S. J. Teat, Y. Q. Cheng, M. D. Frogley, G. Cinque, S. J. Day, C. C. Tang, T. L. Easun, S. Rudić, A. J. Ramirez-Cuesta, S. H. Yang and M. Schröer, *Nat. Mater.*, 2019, **18**, 1358–1365.

15 A. L. Spek, *Acta Crystallogr.*, 2015, **71**, 9–18.

16 Y. L. Wang, Z. Y. Liu, Y. X. Li, Z. L. Bai, W. Liu, Y. X. Wang, X. M. Xu, C. L. Xiao, D. P. Sheng, J. Diwu, J. Su, Z. F. Chai, T. E. Albrecht-Schmitt and S. A. Wang, *J. Am. Chem. Soc.*, 2015, **137**, 6144–6147.

17 X. Han, S. H. Yang and M. Schröer, *Nat. Rev. Chem.*, 2019, **3**, 108–118.

18 X. L. Cui, Q. W. Yang, L. F. Yang, R. Krishna, Z. G. Zhang, Z. B. Bao, H. Wu, Q. L. Ren, W. Zhou, B. L. Chen and H. B. Xing, *Adv. Mater.*, 2017, 1606929.

19 F. Luo, C. S. Yan, L. L. Dang, R. Krishna, W. Zhou, H. Wu, X. L. Dong, Y. Han, T. L. Hu, M. Okeeffe, L. L. Wang, M. B. Luo, R. B. Lin and B. L. Chen, *J. Am. Chem. Soc.*, 2016, **138**, 5678–5684.

20 Z. Z. Xu, X. H. Xiong, J. B. Xiong, R. Krishna, L. B. Li, Y. L. Fan, F. Luo and B. L. Chen, *Nat. Commun.*, 2020, **11**, 3163.

21 C. B. Fan, L. L. Gong, L. Huang, F. Luo, R. Krishna, X. F. Yi, A. M. Zheng, L. Zhang, S. Z. Pu, X. F. Feng, M. B. Luo and G. C. Guo, *Angew. Chem., Int. Ed.*, 2017, **56**, 7900–7906.

22 (*a*) Y. Tao, Y. L. Fan, Z. Z. Xu, X. F. Feng, R. Krishna and F. Luo, *Inorg. Chem.*, 2020, **59**, 11793–11800; (*b*) Y. Tao, R. Krishna, L. X. Yang, Y. L. Fan, L. Wang, Z. Gao, J. B. Xiong, L. J. Sun and F. Luo, *Inorg. Chem. Front.*, 2019, **6**, 2921–2926.

Electronic Supplementary Material (ESI) for Journal of Materials Chemistry A.


# Constructing robust gigantic drum-like hydrophobic [$Co_{24}U_6$] nanocage in metal-organic framework for high-performance $SO_2$ removal at humidity condition

Yaling Fan,[a] Mengjia Yin,[a] Rajamani Krishna,[b] Xuefeng Feng,[a] and Feng Luo[a]*

[a]School of Chemistry, Biology and Materials Science, East China University of Technology, Nanchang 330013, P.R.China

*Corresponding Author(s): Feng Luo: ecitluofeng@163.com
[b]Van't Hoff Institute for Molecular Sciences, University of Amsterdam, Science Park 904, 1098 XH Amsterdam, The Netherlands

**X-ray Crystallography.** X-ray diffraction data of Cage-U-Co-MOF were collected at room temperature on a Bruker Appex II CCD diffractometer using graphite monochromated MoKα radiation (λ=0.71073 Å). The data reduction included a correction for Lorentz and polarization effects, with an applied multi-scan absorption correction (SADABS). The crystal structure was solved and refined using the SHELXTL program suite. Direct methods yielded all non-hydrogen atoms, which were refined with anisotropic thermal parameters. All hydrogen atom positions were calculated geometrically and were riding on their respective atoms. The SQUEEZE subroutine of the PLATON software[15] suite was used to remove the scattering from the highly disordered guest molecules. CCDC 2032794 contains the supplementary crystallographic data of Cage-U-Co-MOF. These data can be obtained free of charge from the Cambridge Crystallographic Data Centre via www.ccdc.cam.ac.uk/data_request/cif.

**Fitting of experimental data on pure component isotherms**

The isotherm data for $SO_2$ and $CO_2$ in Cage-U-Co-MOF at 298 K were fitted with the dual-site Langmuir model, where we distinguish two distinct adsorption sites A and B:

$$q = \frac{q_{sat,A} b_A p}{1 + b_A p} + \frac{q_{sat,B} b_B p}{1 + b_B p}$$

The unary isotherm fit parameters are provided in Table S2.

The isotherm data for $N_2$ in Cage-U-Co-MOF at 298 K was fitted with the 1-site Langmuir model

$$q = q_{sat} \frac{bp}{1 + bp}$$

The 1-site Langmuir fit parameters are provided in Table S3.

**Isosteric heat of adsorption**

The binding energy is reflected in the isosteric heat of adsorption, $Q_{st}$, is calculated from the Clausius-Clapeyron equation

$$Q_{st} = -RT^2 \left( \frac{\partial \ln p}{\partial T} \right)_q$$

For the 1-site Langmuir-Freundlich model the differentiation of the Clausius-Clapeyron equation can be carried out analytically.

**IAST calculations of adsorption selectivities and uptake capacities**

We consider the separation of binary mixtures at 298 K. The adsorption selectivity for $SO_2/CO_2$, $SO_2/N_2$ separation is defined by

$$S_{ads} = \frac{q_1/q_2}{p_1/p_2}$$

**Transient breakthrough simulations**

The performance of industrial fixed bed adsorbers is dictated by a combination of adsorption selectivity and uptake capacity. Transient breakthrough simulations were carried out using the methodology described in earlier publications (*Microporous Mesoporous Mater.* **2014**, *185*, 30-50; *Sep. Purif. Technol.* **2018**, *194*, 281-300; *ACS Omega* **2020**, *5*, 16987−17004). The following two mixtures were investigated.

1/99 $SO_2/CO_2$ mixtures at 298 K,

1/99 $SO_2/N_2$ mixtures at 298 K,

For the breakthrough simulations, the following parameter values were used: length of packed bed, $L$ = 0.3 m; voidage of packed bed, $\varepsilon$ = 0.4; superficial gas velocity at inlet, $u$ = 0.04 m/s.

The *y*-axis is the dimensionless concentrations of each component at the exit of the fixed bed, $c_i/c_{i0}$ normalized with respect to the inlet feed concentrations. The *x*-axis is the *dimensionless* time, $\tau = \frac{tu}{L\varepsilon}$, defined by dividing the actual time, *t*, by the characteristic time, $\frac{L\varepsilon}{u}$.

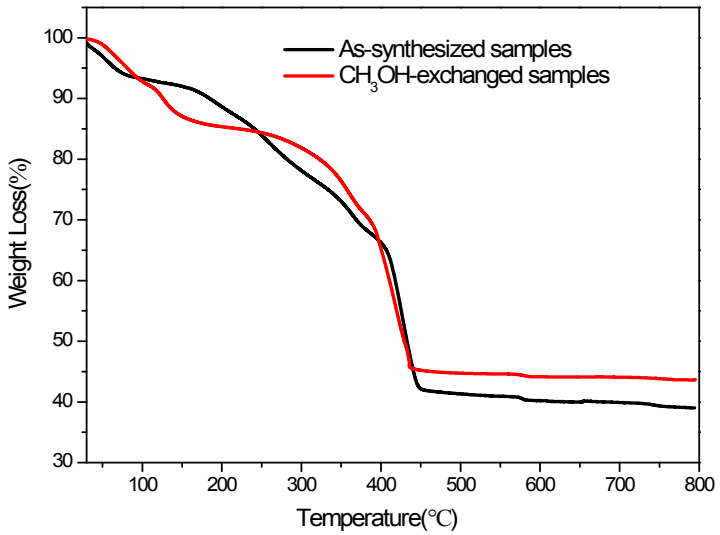


**Fig. S1** The TG plot of **Cage-U-Co-MOF** and the $CH_3OH$-exchanged samples.

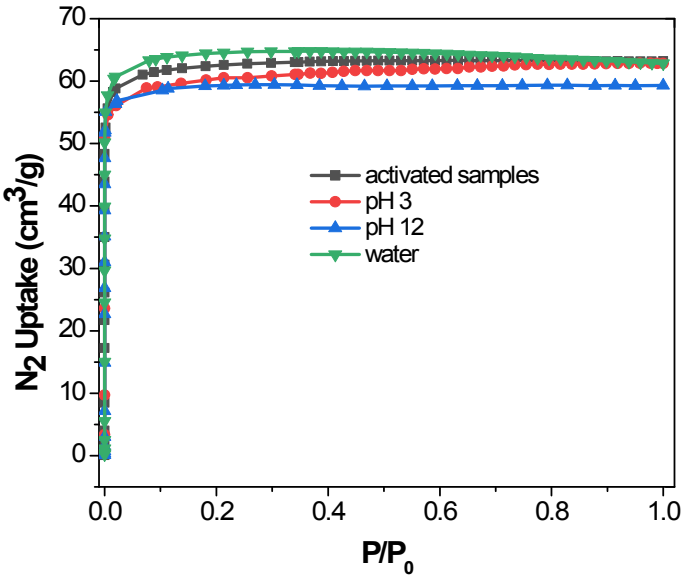


**Fig. S2** A comparison of Ar adsorption at 77 K for the activated samples and the samples after immersing in water and pH=3 and 12 solution. The corresponding BET surface area is 208 $m^2/g$, 212$m^2/g$, 201 $m^2/g$, and 199 $m^2/g$, respectively.

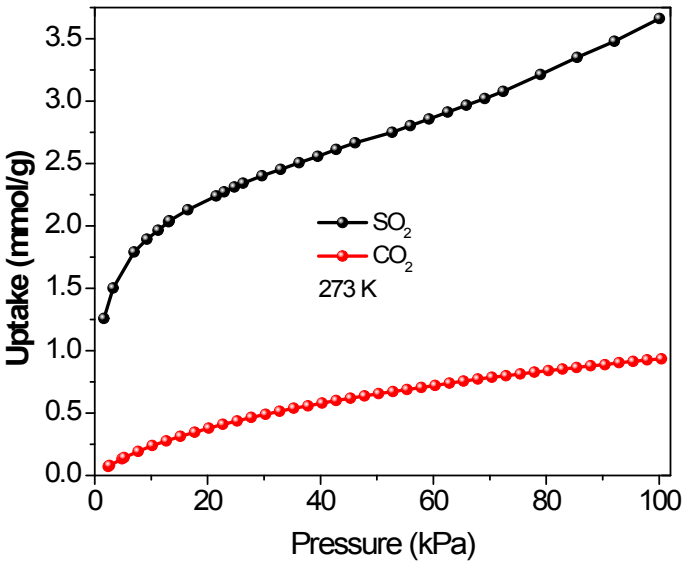


**Fig. S3** The $SO_2$ and $CO_2$ adsorption at 273 K.

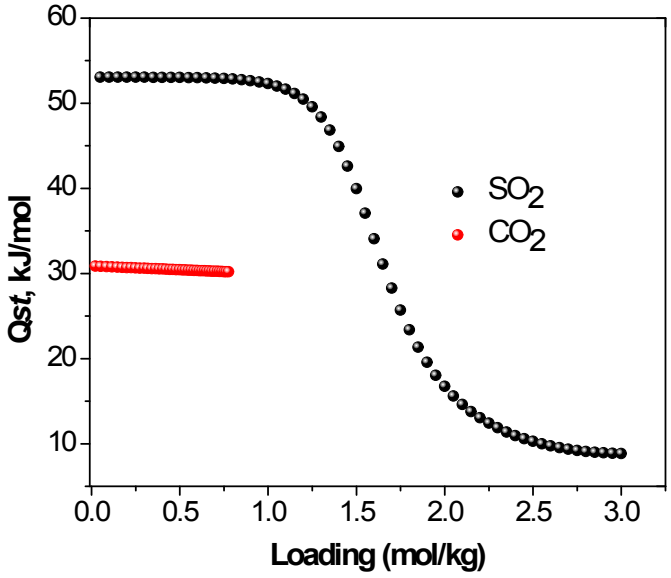


**Fig. S4** The Qst value of $SO_2$ and $CO_2$ for **Cage-U-Co-MOF**.

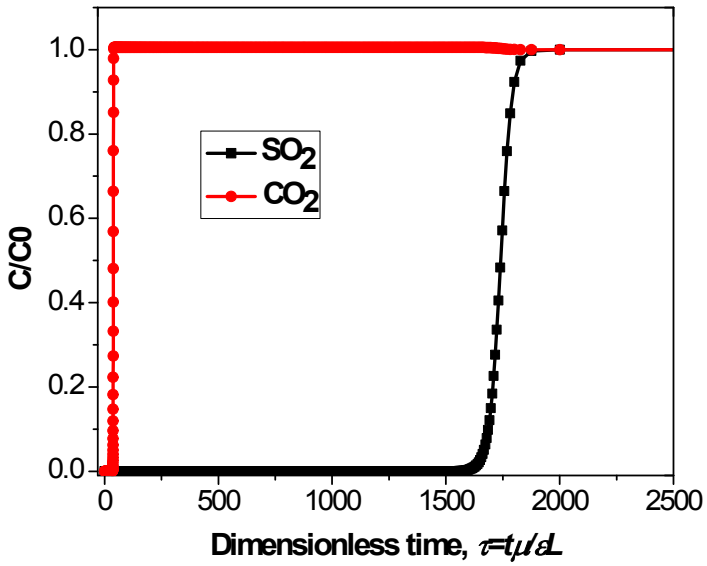


**Fig. S5** The transient breakthrough simulations for a 1:99 v/v $SO_2/CO_2$ mixture based on **Cage-U-Co-MOF** bed.

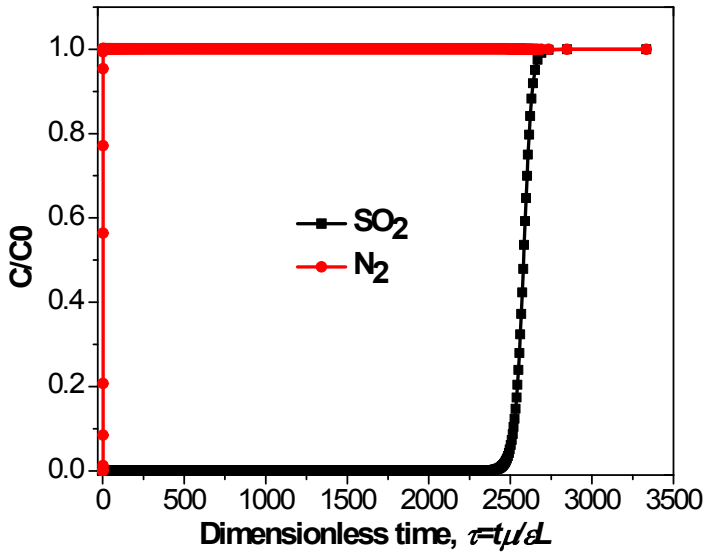


**Fig. S6** The transient breakthrough simulations for a 1:99 v/v $SO_2/N_2$ mixture based on **Cage-U-Co-MOF** bed.

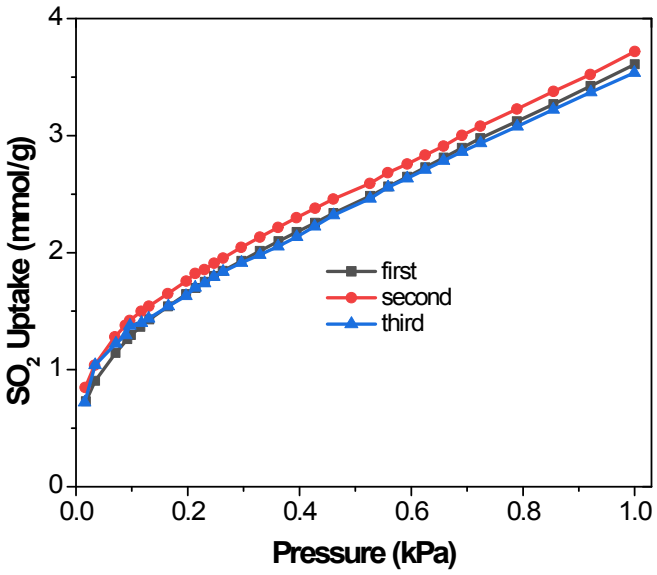


**Fig. S7** Repeating $SO_2$ adsorption test for Cage-U-Co-MOF**.**

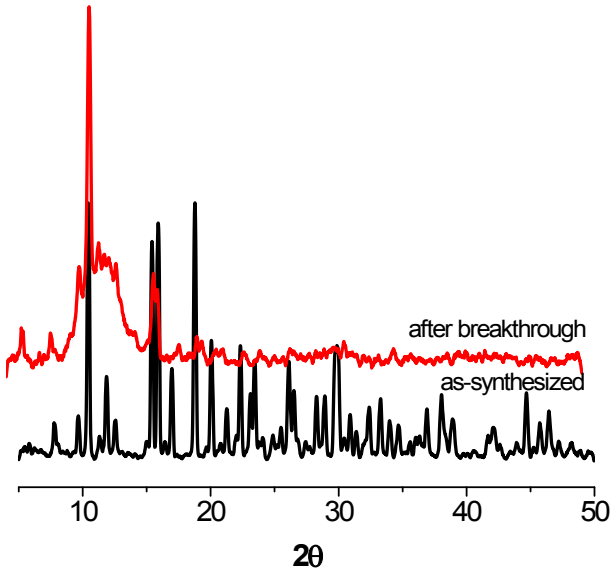


**Fig. S8** A comparison of PXRD patterns of the as-synthesized samples and the samples after all breakthrough experiments.

**Table S1.** A comparison of reported MOFs for $SO_2$ removal.

| MOF tpyes | $SO_2$ adsorption capacity (1 bar, 298 K), mmol/g | $SO_2/CO_2$ selectivity | References |
|---|---|---|---|
| SIFSIX-2-Cu-i | 11.0 | 87.1 | 1 |
| $Ni(bdc)(ted)_{0.5}$ | 9.97 | - | 2 |
| MFM-300(In) | 8.28 | 50 | 3 |
| MFM-202a | 10.2 | - | 4 |
| NOTT-300 (Al) | 7.1 | - | 5 |
| MFM-170 | 17.5 | 28 | 6 |
| MOF-5 | Less than 0.016 | - | 7 |
| IRMOF-3 | 0.094 | - | 7 |
| MOF-74 | 3.03 | - | 7 |
| MOF-199 | 0.5 | - | 7 |
| P(TMGA-co-MBA) | 4.0 | - | 8 |
| Activated Carbon | 3.3 | - | 9 |
| **Cage-U-Co-MOF** | 3.62 | 80.7 | Our work |

"-" denotes the data can not be obtaind from corresponding reference.

1.Cui. X. L.; Yang. Q. W.; Yang. L. F.; Krishna. R.; Zhang. Z. G.; Bao. Z. B.; Wu. H.; Ren. Q.; Zhou. W.; Chen. B. L.; Xing. H. B. Ultrahigh and selective $SO_2$ uptake in inorganic anion-pillared hybrid porous materials. *Advanced Materials*. **2017**. *29*.1606929(1-9).

2. Tan. K.; Canepa. P.; Gong. Q. H.; Liu. J.; Johnson. D. H.; Dyevoich. A.; Thallapally. P. K.; Thonhauser. T.; Li. J.; Chabal. Y. J. Mechanism of preferential adsorption of $SO_2$ into two microporous paddle wheel frameworks $M(bdc)(ted)_{(0.5)}$. *Chemistry of Materials*. **2013**. *25*. 4653-4662.

3. Savage. M.; Cheng .Y. Q.; Easun. T. L.; Eyley. J. E.; Argent.S. P.; Warren. M. R.; Lewis. W.; Murray. C.; Tang. C. C.; Frogley. M. D.; Cinque G.; Sun. J. L.; Rudic´. S.; Murden R. T.; Benham. M. J.; Fitch. A. N.; Blake. A. J.; Ramirez-Cuesta. A. J.; Yang. S. H.; Schroder. M. Selective Adsorption of Sulfur Dioxide in a Robust Metal–Organic Framework Material. *Advanced Materials*.

**2016**. *28*. 8705-8711.

4. Yang. S. H.; Liu. L. F.; Sun. J. L.; Thomas. K. M.; Davies A. J.; George. M. W.; Blake. A. J.; Hill. A. H.; Fitch. A. N.; Tang. C. C. , Chroeder. M. Irreversible network transformation in a dynamic porous host catalyzed by sulfur dioxide. *Journal of the American Chemical Society*. **2013**. *135*. 4954-4957.

5. Yang. S. H.; Sun. J. L.; Ramirez-Cuesta. A. J.; Callear. S. K.; David. W. F.; Anderson. D. P.; Newby. R.; Blake1. A. J.; Parker. J. E.; Tang. C. C.; Schro¨der1. M. Selectivity and direct visualization of carbon dioxide and sulfur dioxide in a decorated porous host. *Nature chemistry.* **2012**. *4*.887-894.

6. Smith. G. L.; Eyley. J. E.; Han. X.; Zhang. X. R.; Li. J. N.; Jacques. N. M.; Godfrey. H. G. W.; Argent. S. P.; McPherson. L. J. M.; Teat. S. J.; Cheng Y. Q.; Frogley. M. D.; Cinque. G.; Day S. J.; C. C. Tang.; Easun . T. L.; Rudić. S.; Ramirez-Cuesta . A. J.; Yang. S.H.; Schro¨der1. M. Reversible coordinative binding and separation of sulfur dioxide in a robust metal–organic framework with open copper sites. *Nature Materials.* **2019**. *18*. 1358-1365.

7. Britt. D.; Tranchemontagne. D.; Yaghi O. M. Metal-organic frameworks with high capacity and selectivity for harmful gases. *Proceedings of the National Academy of Sciences of the United States of America*. **2008**. *105*. 11623-11627.

8. Wu. L. B.; An. D.; Dong. J.; Zhang. Z. M.; Li. B. G.; Zhu. S. P. Preparation and SO2 Absorption/Desorption Properties of Crosslinked Poly(1,1,3,3-Tetramethylguanidine Acrylate) Porous Particles. *Macromolecular Rapid Communications*. **2006**. *37*.1949-1954.

9. Yi. H. H.; Wang. Z. X.; Liu. H.Y.; Tang X. L.; Ma. D.; Zhao. S. Z.; Zhang. B. W.; Gao. F. Y.; Zuo Y. R. Adsorption of $SO_2$, NO, and $CO_2$ on Activated Carbons: Equilibrium and Thermodynamics . *Journal of Chemical & Engineering Data.* **2014**. *59*. 1556-1563.

**Table S2.** Dual-site Langmuir parameter fits for $SO_2$ and $CO_2$ in Cage-U-Co-MOF at 298 K.

| | Site A | | Site B | |
|---|---|---|---|---|
| | $q_{A,sat}$ mol $kg^{-1}$ | $b_A$ $Pa^{-1}$ | $q_{B,sat}$ mol $kg^{-1}$ | $b_B$ $Pa^{-1}$ |
| $SO_2$ | 11 | 2.875E-06 | 1.1 | 8.548E-04 |

| | | | | |
|---|---|---|---|---|
| $CO_2$ | 0.2 | 5.562E-06 | 2 | 5.441E-06 |

**Table S3.** 1-site Langmuir parameter fits for $N_2$ in Cage-U-Co-MOF at 298 K.

| | $q_{sat}$<br>mol $kg^{-1}$ | $b$<br>$Pa^{-1}$ |
|---|---|---|
| $N_2$ | 0.15 | 3.21095E-06 |